Electronic Supplementary Material (ESI) for Journal of Materials Chemistry A.
This journal is © The Royal Society of Chemistry 2023

Supporting information

Enhancing Energy Transfer by Regulating Electron Transport Pathways in Semiconductor Metal-Organic Framework

Peng-Da Liu[a], Yuan Chen[a,*], Ao-Gang Liu[a], Zi-Tong Chen[a], Bao Li[a,*]

[a] Key Laboratory of Material Chemistry for Energy Conversion and Storage, Semiconductor chemistry center, School of Chemistry and Chemical Engineering, Hubei Key Laboratory of Bioinorganic Chemistry&Materia Medica, Huazhong University of Science and Technology, Wuhan, Hubei 430074, People's Republic of China.Email: chenyuan122800@163.com; libao@hust.edu.cn

Experimental

1. Chemicals

All materials used include 1,4,5,8-naphthalene tetracarboxylic anhydride, 4-Amino-4H-1,2,4-triazole, DMF, $FeCl_3$, acetonitrile,5,5-dimethyl-1-pyrroline-N-oxide (DMPO), cysteine, EDTA-2Na,

2,2,6,6-Tetramethylpiperidine (TEMP), tert-butanol, p-benzoquinone (p-BQ) are of analytical grade and are used directly without further purification. Tetracycline hydrochloride (TC-HCl) was purchased from Aladdin Co., Ltd. (Shanghai, China). Sulfamethoxazole (SMX) was purchased from Heowns Co., Ltd. (Tianjin, China). The ultrapure water used in the experiments was experimentally homemade.

2. Synthesis of Fe-MOF

According to the design concept, the DBPT ligand was synthesized using a simple method (Fig. S4). The black crystal HUST-30 was synthesized through a hydrothermal method. 15 mg of the DBPT ligand and 10 mg of $FeCl_3$ were added to a mixed solution containing 3 mL DMF and 200 μL of tetrafluoroboric acid in a heating vessel. The mixture was sonicated to ensure uniform dispersion and dissolved, then reacted in a 120°C oven for 72 h. After cooling to room temperature, a black precipitate was observed. The solid was separated by centrifugation, washed with DMF three times, activated by washing with acetonitrile, and finally vacuum-dried at 60°C.

3. Characterization

At room temperature, the X-ray diffraction (PXRD) pattern of the sample was measured using Cu-*K*α radiation (λ=1.5406Å) on a Rigaku Smart Lab-SE X-ray powder diffractometer supplied by Japan RIKEN Corporation. X-ray photoelectron spectroscopy (XPS) was characterized using a Thermo Fisher Scientific K-alpha 250Xi spectrometer from the USA. The morphology and microstructure of the sample were measured via scanning electron microscopy (SEM). Fourier transform infrared (FTIR) spectra were obtained using a Bruker ALPHA II FTIR spectrometer. Thermal gravimetric analysis (TGA) was conducted using a Perkin Elmer diamond differential thermal analyzer (TGA 55) in the air at room temperature to 800℃. UV–vis diffuse reflectance spectra (DRS) were recorded using a Shimadzu UV-3600 recording

spectrophotometer equipped with an integrating sphere and employing BaSO4 as a reference. Electron paramagnetic resonance (EPR) signals were determined under visible light using a Bruker EMX microspectrometer. High-performance liquid chromatography (HPLC) was performed using a Thermo Fisher Scientific UltiMate 3000 HPLC. Relevant electrochemical tests were conducted on a CHI660E workstation (Shanghai Chenhua Instruments Co., Ltd.) using a three-electrode electrochemical cell with a working electrode, a platinum counter electrode, and an Ag/AgCl reference electrode in the dark. A 0.5 M Na_2SO_4 solution was used at frequencies 1200 and 1500. A working electrode was prepared by coating the sample onto a glassy carbon electrode. Mott-Schottky measurements were carried out using impedance potential models to evaluate the valence band position of Fe MOF catalysts.

4 Photocatalytic experiments

Fe-MOF was tested by photocatalytic degradation of tetracycline hydrochloride (TC-HCl) using the PCX50B Discover multichannel photocatalytic reaction system with an LED white light lamp (380-800 nm, 5 W) as the visible light source. A certain amount of photocatalyst (5 mg) was added to 40 mL of aqueous TC solution (350 mg L^{-1}) under magnetic stirring (280 rpm). First, the solution was stirred in the dark for 1 h to achieve the adsorption equilibrium of the catalyst. Subsequently, an amount of H_2O_2 (10 μL,2.5 mM) was added to the mixture and the LED light was turned on for irradiation. Then, the samples were extracted at predetermined time intervals and filtered through a 0.22 μm syringe filter to remove the solid photocatalyst. Finally, the concentration of the TC was determined using HPLC.

To investigate the effect of influencing parameters on the degradation of TC-HCl, the experimental conditions were adjusted to: HUST-30 concentrations (0.075, 0.125, 0.25, and 0.375 g/L); hydrogen peroxide concentrations (1.25, 2.5, 3.75, 5 mM). The initial pH values were adjusted with HCl and NaOH (2.0, 4.0, 6.0, 8.0, and 10.0).

To evaluate the stability and reusability of the photocatalysts, experiments were performed in five consecutive cycles using the recovered catalysts. After each reaction, the solid photocatalyst was collected by centrifugation and washed thoroughly with ultrapure water and ethanol for the next test.

5 Analytical methods

Degradation efficiency (%) = $[(C_0\text{-}C_t)/C_0] \times 100$, where C_0 is the initial concentration of TC and C_t is the concentration of TC at time t during the reaction. The residual concentration of TC was measured by HPLC. The concentration of TC in the solution was detected by high pressure liquid chromatography using a C18 column (250 mm × 4.6 mm, 5 μm) and a UV-Vis detector. The concentration of tetracycline hydrochloride was measured at its maximum absorption wavelengths of 358 nm. 70% aqueous formic acid at 0.1% and 30% acetonitrile were used as the mobile phases with a flow rate of 1 mL/min and a column temperature of 25 ℃, and the sample injection volume was 20 μL.

6 X-Ray Structural Determination.

Diffraction data for Fe-MOF (0.2 × 0.05 × 0.05 mm) was collected via Bruker Venture using Cu-K_α (λ = 1.54178 Å) radiation at 173 K in Shanghai Synchrotron Radiation Facility. The structures of complex was solved by direct methods, and the non-hydrogen atoms were located from the trial structure and then refined anisotropically with SHELXTL using a full-matrix leastsquares procedure based on F^2 values. The hydrogen atom positions were fixed geometrically at calculated distances and allowed to ride on the parent atoms. CCDC-2259680 for Fe-MOF contain the supplementary crystallographic data for this paper. These data can be obtained free of charge from The Cambridge Crystallographic Data Centre via http://www.ccdc.cam.ac.uk/datarequest/cif.

7 Theoretical calculations

Density functional theory (DFT) calculations were carried on Materials Studio 2020 package. The structures of intermediates were optimized by Dmol^3 module, following by the frequency calculation to obtain zero point vibration energy and Gibbs free energy. The generalized gradient approximation (GGA) with the Perdew-Burke-Ernzerhof (PBE) function and TS for DFT-D correction were employed. The convergence tolerance of energy, force and displacement convergence were set as 1×10^{-4} Ha, 2×10^{-3} Ha, and 5×10^{-3} Å, respectively. The core treatment was chosen as the effective core potential (ECP), and the electron treatment was performed by double

numerical plus d-functions (DNP) basis set.

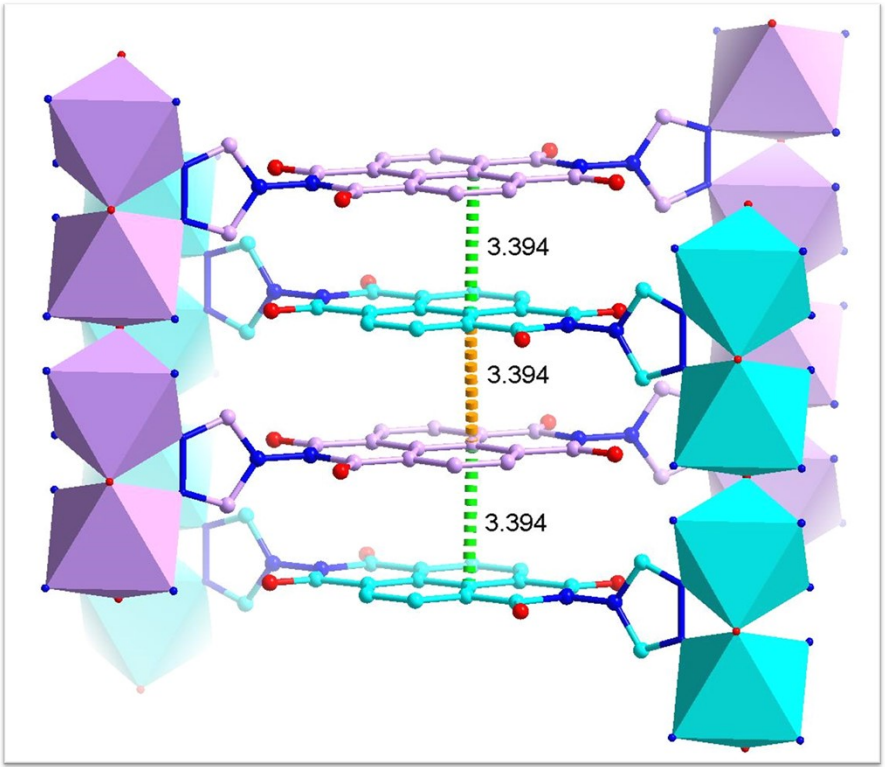

Fig. S1 Interaction between different framework in HUST-30

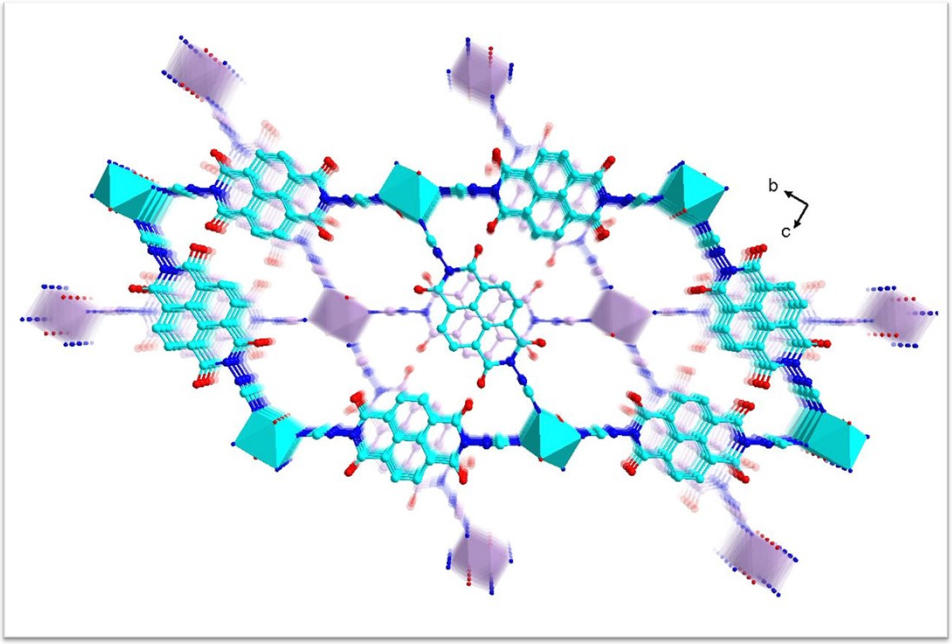

Fig. S2 Two-fold interpenetrating structure of HUST-30

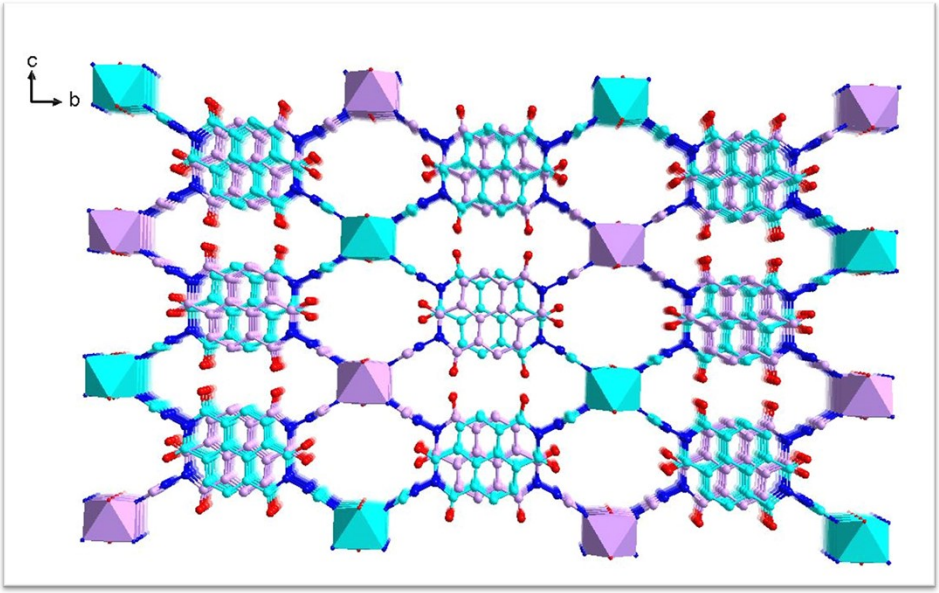

Fig. S3 Three-dimensional structure of HUST-30

Table S1. Selected bond length of Fe-MOF

	Fe-MOF
Empirical formula	C_{18} H_8 Fe N_8 O_5
Formula weight	472.17
Crystal system	orthorhombic
Space group	*C*mme
a/Å	6.6655(12)
b/Å	30.475(6)
c/Å	8.7911(18)
α/°	90
β/°	90
γ/°	90
Volume/Å3	1785.7(6)
Z	24
ρcalcg/cm^3	2.207
μ/mm^{-1}	4.777
2Θ range for data collection/°	2.672 to 46.402
Index ranges	$-7 \le h \le 7$, $-33 \le k \le 33$, $-9 \le l \le 9$
Reflections collected	8800
Independent reflections	720 [R_{int} = 0.0959, R_{sigma} = 0.0389]

Data/restraints/parameters	720/0/94
Goodness-of-fit on F^2	1.189
Final R indexes [I>=2σ (I)]	R_1 = 0.0685, wR_2 = 0.2337
Final R indexes [all data]	R_1 = 0.0742, wR_2 = 0.2397

Table S2. Selected bond length of Fe-MOF

Atom	Atom	Atom	Length/Å
Fe01	O002[1]	C00F	1.281(8)
Fe01	O002	C00F	1.356(8)
Fe01	N006[1]	C00F[4]	1.357(8)
Fe01	N006[2]	C009[5]	1.409(12)
Fe01	N006[3]	C00B[5]	1.455(12)
Fe01	N006	C00E	1.395(12)
O003	C00B	C009[5]	1.436(17)
O004	C00C	C00A	1.396(12)
N005	N007	C00C	1.451(11)
N005	C00B	C00D	1.393(12)
N005	C00C	C00E	1.362(12)
N006	N006[4]		

13/2-X,3/2-Y,2-Z; 2+X,3/2-Y,+Z; 33/2-X,+Y,2-Z; 41-X,+Y,+Z; 51-X,1-Y,1-Z

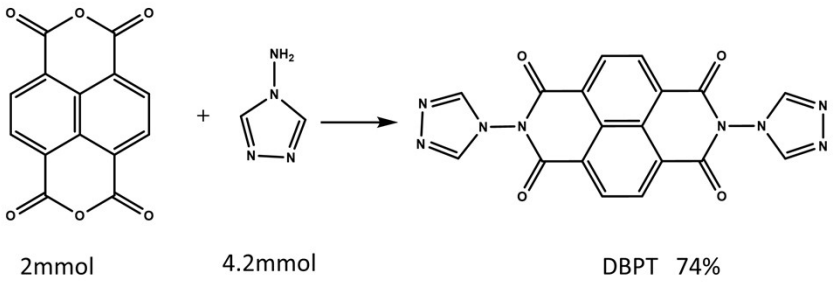

Fig. S4 Synthesis of DBPT: Under room temperature, 1,4,5,8-naphthalene tetracarboxylic dianhydride(2mmol) and 4-Amino-4H-1,2,4-triazole(4.2mmol) were added to a round-bottom flask, followed by the addition of 30 mL DMF. The mixture was stirred and heated to reflux at 150°C for 36 h. After cooling the solution, a large amount of water and methanol were added, resulting in the precipitation of a brown-red solid. The solid was filtered, washed, and dried to obtain the DBPT ligand.

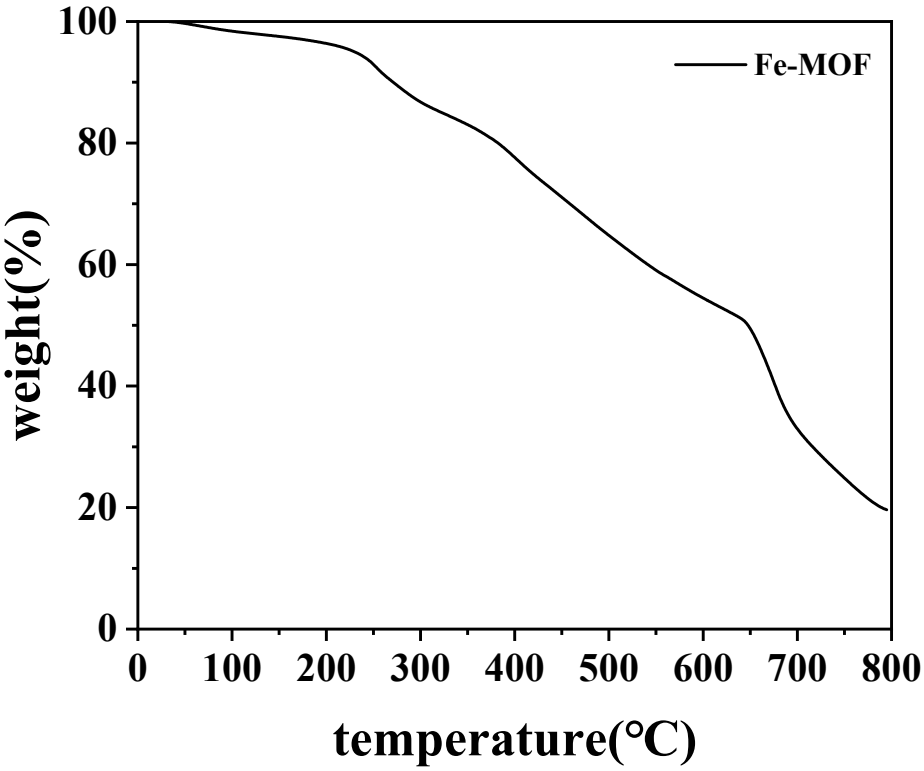

Fig. S5 TGA curve of HUST-30.

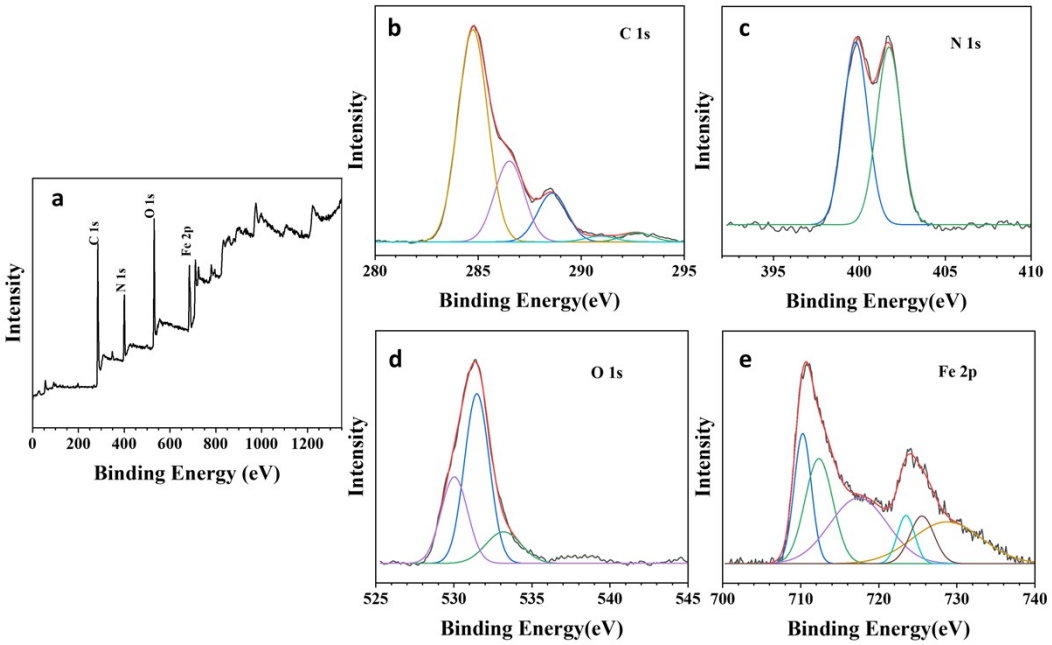

Fig. S6 XPS spectra of HUST-30: (a) full spectra of samples; (b) C 1s peaks; (c) N 1s peaks; (d) O 1s peaks; (d) Fe 2p peaks.

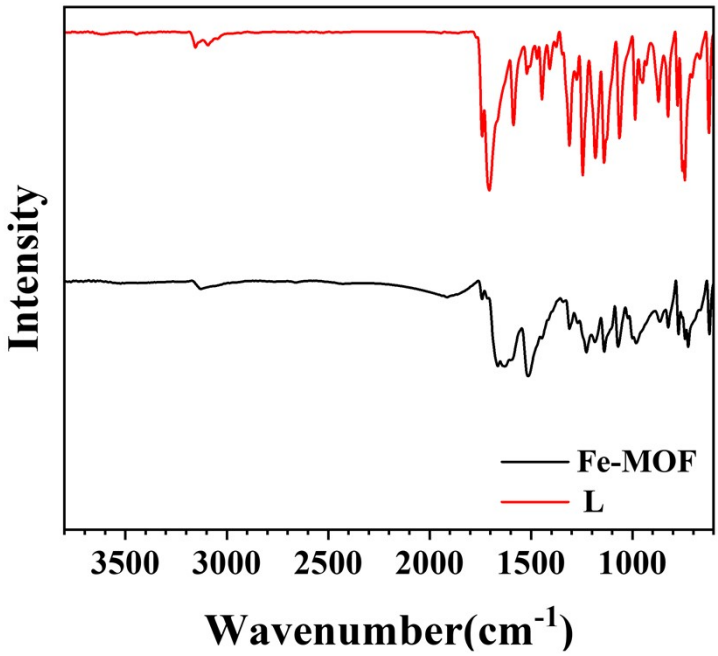

Fig. S7 FTIR of HUST-30

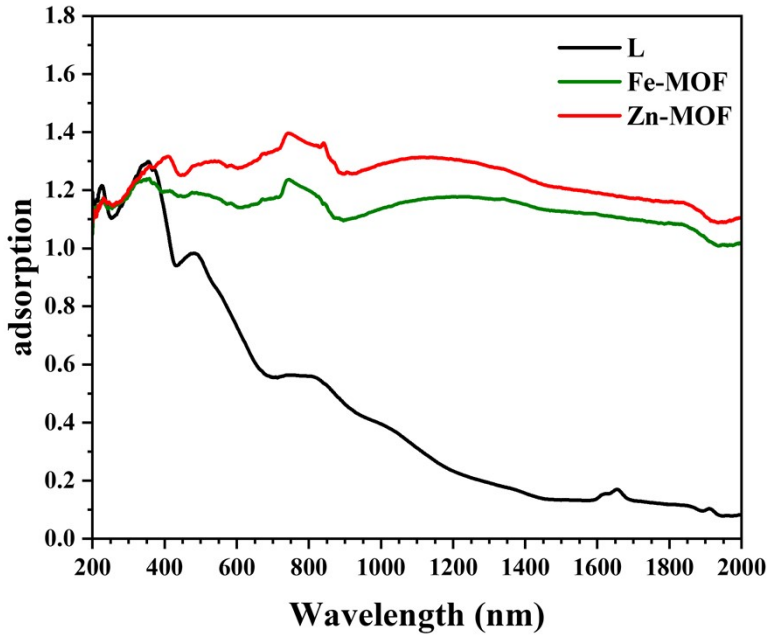

Fig. S8 UV–vis DRS spectra of HUST-30(Fe-MOF), HUST-32(Zn-MOF) and DBPT (L)

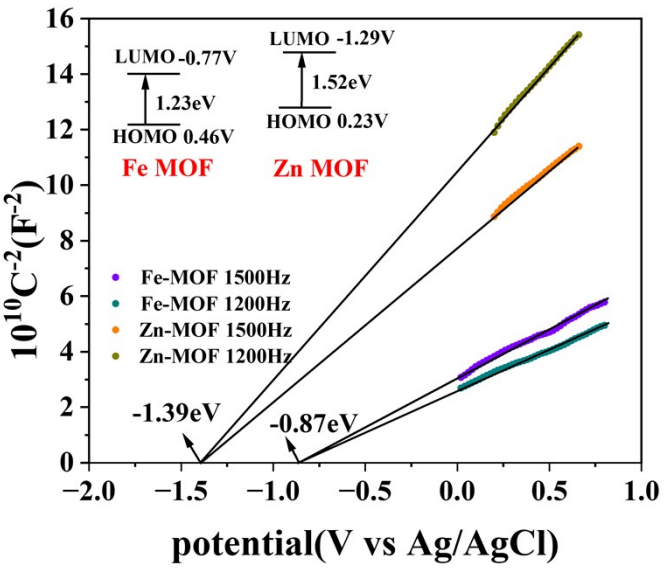

Fig. S9 Mott-Schottky plots of Fe-MOF and Zn-MOF

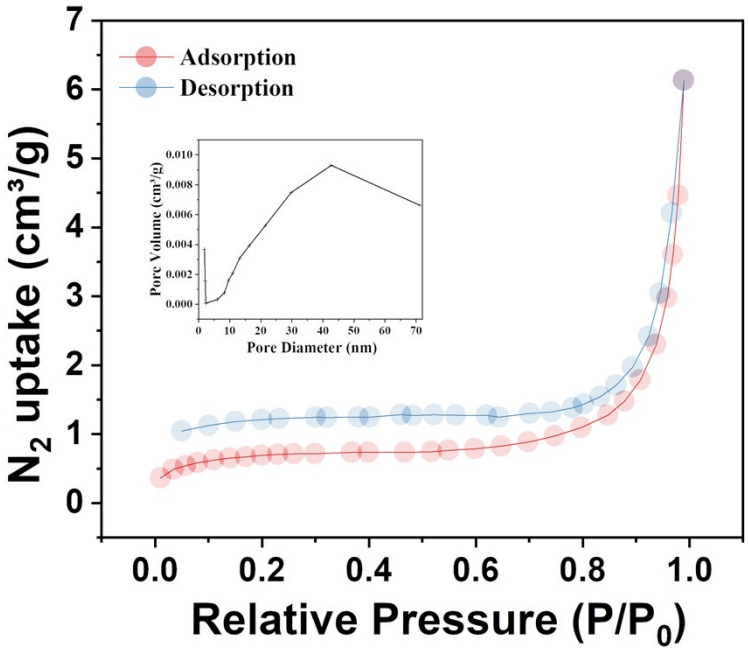

Fig. S10 N_2 adsorption/desorption at 77 K for HUST-30

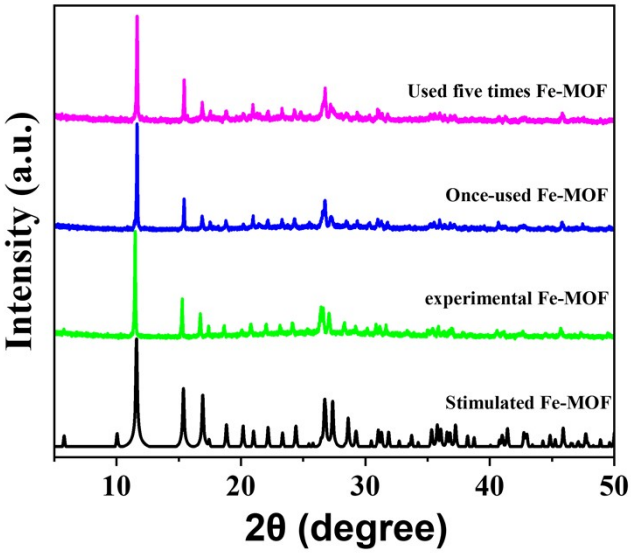

Fig. S11 XRD patterns of HUST-30 before and after used

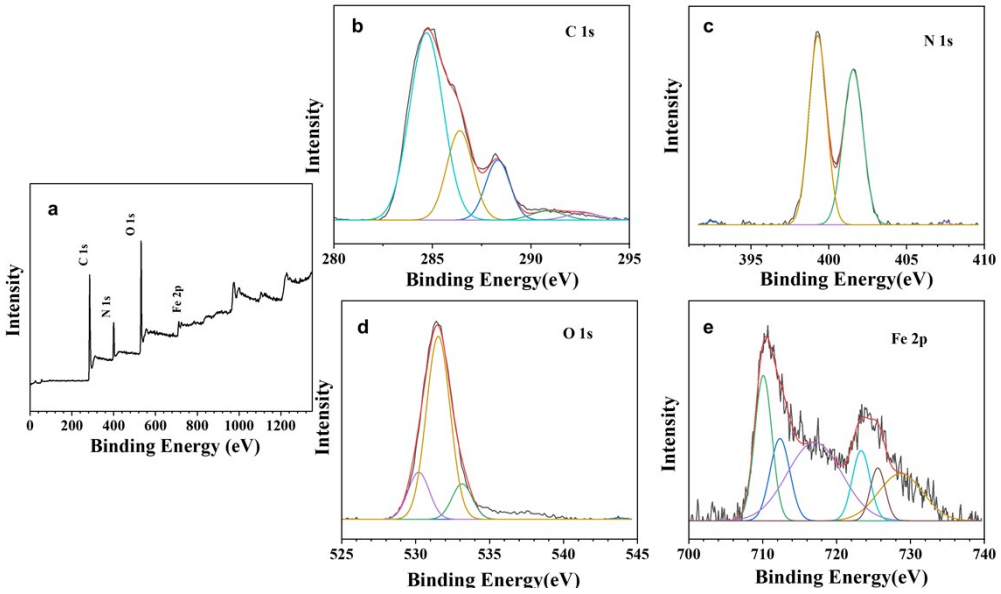

Fig. S12 XPS spectra of used HUST-30: (a) full spectra of samples; (b) C 1s peaks; (c) N 1s peaks; (d) O 1s peaks; (d) Fe 2p peaks.

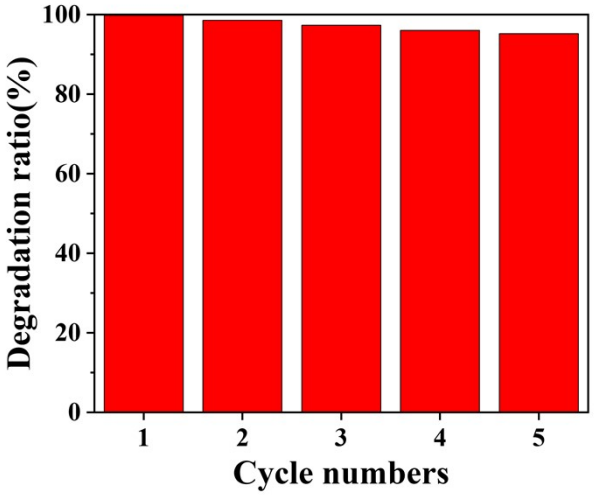

Fig. S13 catalytic reusability of HUST-30

Table S3. Comparison of the photocatalytic performance of HUST-30 with other Fe-based photocatalysts in the reported literatures

Catalyst	catalyst dosage	H_2O_2 (mM)	t (min)	SMX (mg/L)	Removal efficiency (%)	Ref.
HUST-30	**0.125g/L**	**3.75**	**120**	**100**	**96.5**	**this work**
Fe_xCu_{1-x}(BDC)	0.5	6	120	20	100.0	[1]
MIL-53(Fe)	2mmol/L	2	120	0.2	96.0	[2]
PPyC@Py-MIL(Fe)	1mmol/L	3.3	60	100	93.0	[3]
BUC-21(Fe)	0.3g/L	2.94	25	5	100.0	[4]
CUCs-MIL-88B-Fe/Ti_3C_2	0.5g/L	10	120	30	99.0	[5]

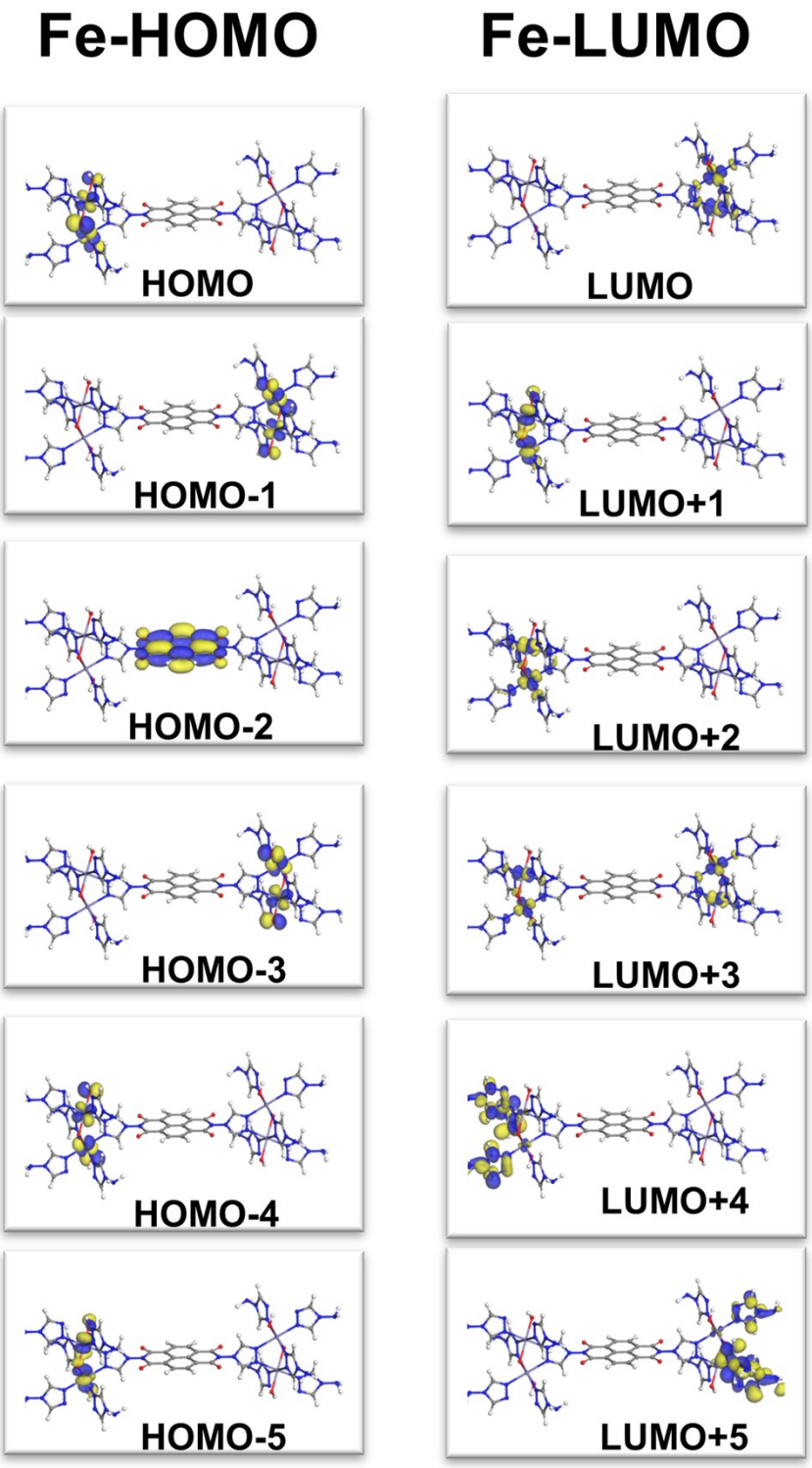

Fig. S14 Energy level orbital diagram of HUST-30

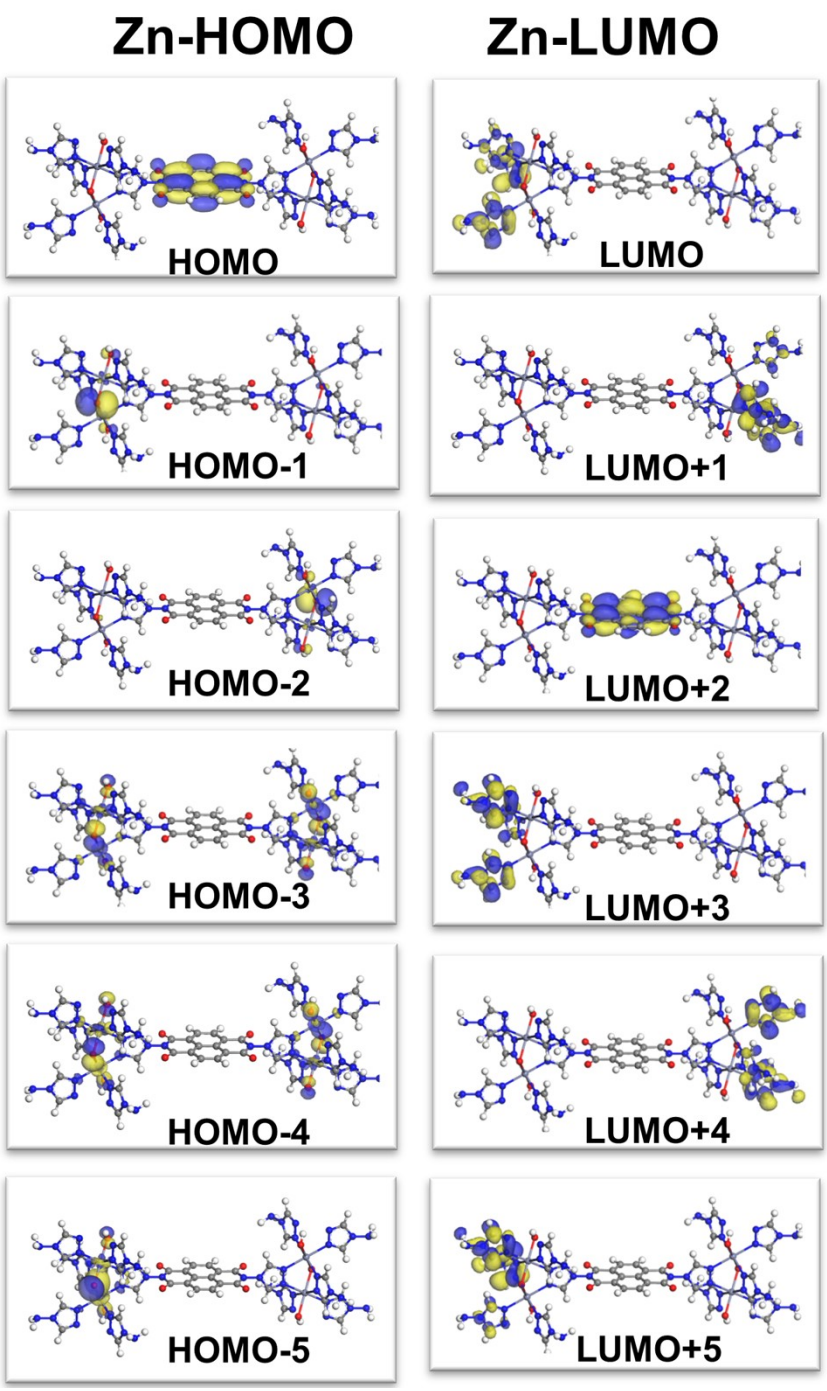

Fig. S15 Energy level orbital diagram of HUST-32

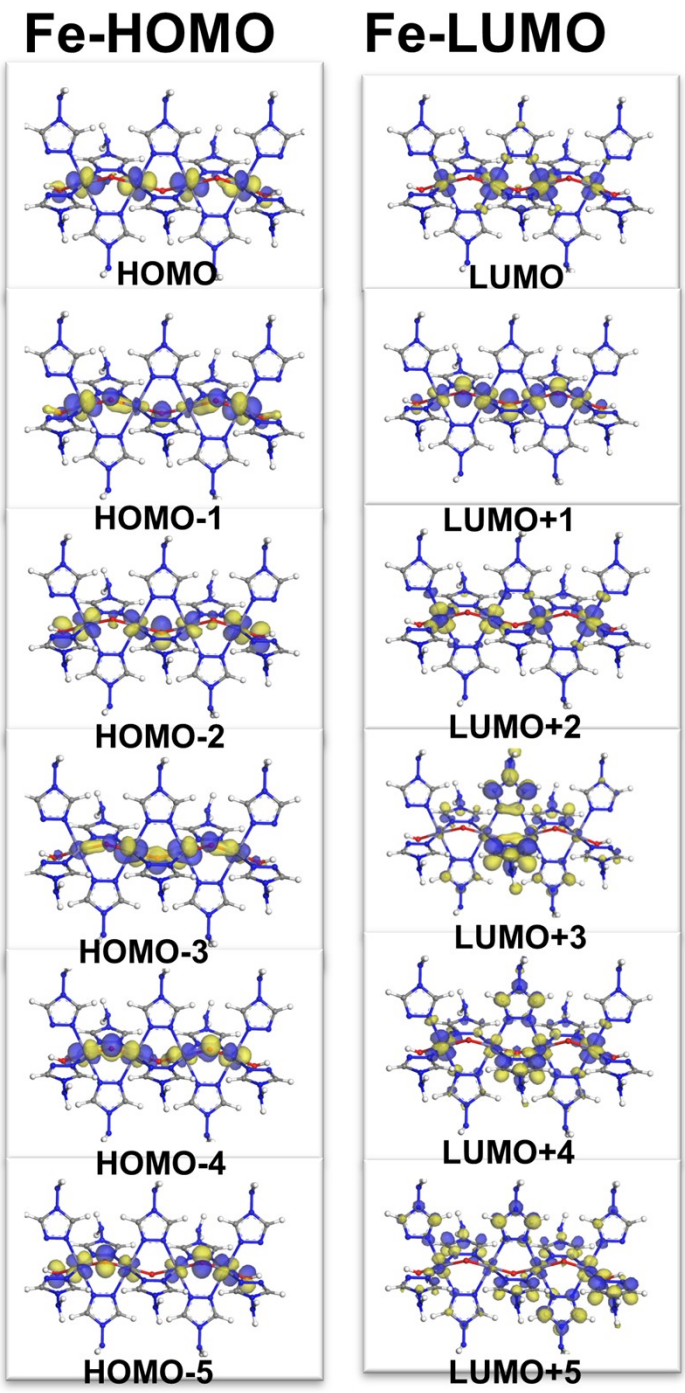

Fig. S16 Energy level orbital diagram of Fe-O-trizaole chain

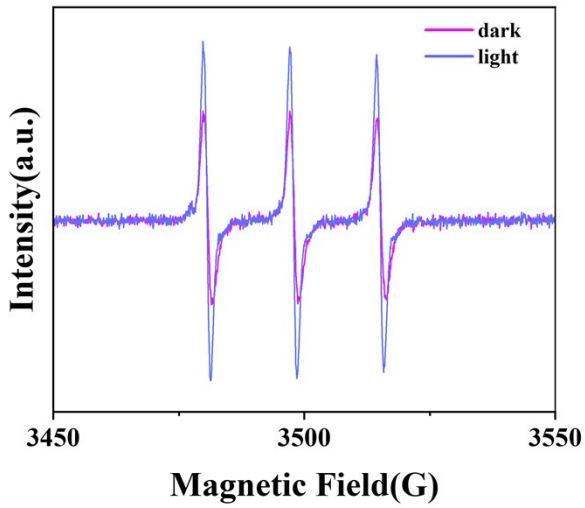

Fig. S17 EPR spectra of TEMP-$^1O_2$

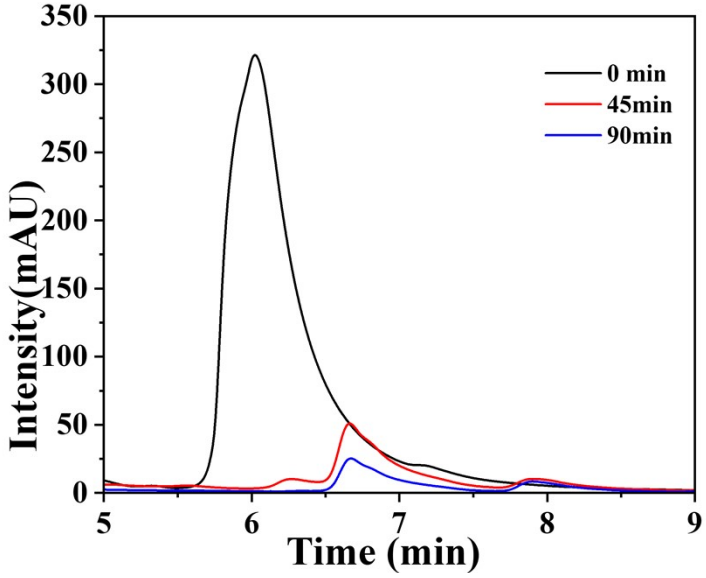

Fig. S18 HPLC spectra of degradation SMX from 0 min to 90 min. Reaction conditions: 30w 850 nm LED lamp ; TC (350 mg/L); SMX (150 mg/L); HUST-30 (0.125 g/L); H_2O_2 (3.75 mM).

Reference

[1] J. Tang, J. Wang, Iron-copper bimetallic metal-organic frameworks for efficient Fenton-like degradation of sulfamethoxazole under mild conditions, Chemosphere, 241 (2020) 125002.

[2] G.A. Ortega-Moreno, S.C. Ayala-Durán, B.P. Barbero, G.E. Narda, M.C. Bernini, R.F. Pupo Nogueira, Photo-Fenton degradation of sulfamethoxazole using MIL-53(Fe) under UVA LED irradiation and natural sunlight, Journal of Environmental Chemical Engineering, 10 (2022) 107678.

[3] H. He, Y. Wang, J. Li, S. Jiang, S. Sidra, W. Gong, Y. Tang, Y. Hu, R. Wei, D. Yang, X. Li, Z. Zhao, Confined conductive and light-adsorbed network in metal organic frameworks (MIL-88B(Fe)) with enhanced photo-Fenton catalytic activity for sulfamethoxazole degradation, Chem. Eng. J., 427 (2022) 131962.

[4] F.-X. Wang, C.-C. Wang, X. Du, Y. Li, F. Wang, P. Wang, Efficient removal of emerging organic contaminants via photo-Fenton process over micron-sized Fe-MOF sheet, Chem. Eng. J., 429 (2022) 132495.
[5] M. Ahmad, X. Quan, S. Chen, H. Yu, Tuning Lewis acidity of MIL-88B-Fe with mix-valence coordinatively unsaturated iron centers on ultrathin Ti_3C_2 nanosheets for efficient photo-Fenton reaction, Applied Catalysis B: Environmental, 264 (2020) 118534.